Title: Electronic Structure and X-Ray Photoemission Spectra of MPtSn (M = Ti, Zr, Hf)

Author: J.A. Morkowski, A. Szajek, Grażyna Chełkowska, Anna Bajorek, R. Troć

Citation style: Morkowski J.A., Szajek A., Chełkowska Grażyna, Bajorek Anna, Troć R. (2009). Electronic Structure and X-Ray Photoemission Spectra of MPtSn (M = Ti, Zr, Hf). "Acta Physica Polonica A" (Vol. 115, nr 5 (2009), s. 935-940).

Electronic Structure and X-Ray Photoemission Spectra of MPtSn (M = Ti, Zr, Hf)

J.A. Morkowski[a], A. Szajek[a,*], G. Chełkowska[b], A. Bajorek[b] and R. Troć[c]

[a]Institute of Molecular Physics, Polish Academy of Sciences
M. Smoluchowskiego 17, 60-179 Poznań, Poland

[b]A. Chełkowski Institute of Physics, Silesian University
Uniwersytecka 4, 40-007 Katowice, Poland

[c]W. Trzebiatowski Institute of Low Temperature and Structure Research
Polish Academy of Sciences, P.O. Box 1410, 50-950 Wrocław, Poland

(Received November 4, 2008; revised version December 14, 2008)

The electronic structures of the half-Heusler isostructural compounds TiPtSn, ZrPtSn and HfPtSn were calculated and measured applying the X-ray photoemission spectroscopy. The (Ti, Zr, Hf)PtSn compounds have gaps between the occupied valence band and the empty conduction band, calculated as about 0.75, 1.12, and 1.09 eV, respectively. The calculations were done by the full-potential local orbitals method in the framework of the local spin-density approximation and partly also by the full-potential linear muffin-tin orbitals method by the LmtART code. Experimental X-ray photoemission spectra were measured using photons of energy of 1486.6 eV. The experimental and calculated spectra match quite well except a small shift in the energy scale.

PACS numbers: 71.20.−b, 82.80.Pv

1. Introduction

A large class of intermetallic ternary compounds with general chemical formula MTSn (M = Ti, Zr, Hf, U, Th, T = mainly 3*d* metal like Ni) and being the so-called half-Heusler phases, has recently attracted a great deal of attention. A remarkable feature of these materials is that, despite they all consist of metallic elements, they are semiconductors. Just the presence of vacancies in the crystal lattice of the cubic MgAgAs type structure [1, 2] gives rise to the formation of a narrow gap near the Fermi level of the size several tenths electron volts. At the same time this feature may lead to high value of the Seebeck coefficient, even of the order of -300 μV/deg [3], and such materials are considered as attractive candidates for thermoelectric applications [4]. In turn the full Heusler phases AT_2Sn (cubic $AlCu_2Mn$ type structure) show usually metallic-like conduction. In the cubic MgAgAs type structure, having usually electron valence concentration $z = 16$–20 electrons per formula unit, where one of the sublattices is entirely vacant, the A atoms ideally occupy each second rock-salt cube. Compounds considered in this work have $z = 18$, i.e. the most favorable number of valence electrons to form the narrow-gap semiconductors [5].

As always it was observed for half-Heusler phases, the properties are strongly dependent on the degree of crystallographic order, particularly involving site interchange, being clear inherent properties of these systems. Usually, sample homogeneity has a profound effect on the electrical transport observed in the half-Heusler phases.

Measurements of transport properties in the past were made mainly on polycrystalline samples and it was found that impurities and defects play a pronounced role in determination of the low temperature properties. Only recently the transport behavior for TiNiSn, HfNiSn and TiPtSn were reported by Ahilan et al. [5], which were measured on single-crystalline samples. All of them show the temperature dependences of the electrical resistivity having the behavior typical of *n*-type semiconductors. The higher temperature transport gaps are very small: 26 meV for HfNiSn, 28 meV for TiPtSn and 79 meV for TiNiSn. All these magnitudes of the gaps are considerably smaller than the values previously reported for polycrystals [2] or single crystal TiNiSn [6] carried out to temperatures as high as 1000 K. Another indication of a band gap in these phases is the extremely low density of carriers, obtained from the Hall effect measurements [6].

The single-crystalline gaps are also smaller than the indirect gaps of 0.5 eV found in electronic structure calculations made for TiNiSn and HfNiSn by applying a pseudopotential method [7]. These calculations support the view that the semiconducting behavior found for

* corresponding author; e-mail: szajek@ifmpan.poznan.pl

MNiSn (M = Ti, Zr, Hf) is an intrinsic feature, evidencing indirect gaps between the Γ and X points in each compound. It appears that the gap is first of all dependent on the strength of M–Sn *pd* hybridization [7]. Ślebarski et al. [8] have studied electronic structures of TiNiSn and ZrNiSn in the local spin density approximation (LSDA) by the self-consistent tight binding linear muffin-tin orbital TB-LMTO method within the atomic spheres approximation (ASA). The results of computations were compared to the UPS and XPS experimental data obtaining fair good agreement between the theoretical and experimental data. Also in these studies a strong hybridization, the gap formation at the Fermi energy and the gap in the middle of the valence band have been demonstrated and discussed. The detailed analysis of electronic structure of a series of half-Heusler compounds, including TiNiSn or ZrNiSn, has recently been done by Nanda and Dasgupta [9] who have applied the full potential LMTO (FP-LMTO) and TB-LMTO methods. This analysis leads the authors to the conclusion that the covalent hybridization of the transition element (here Ni) with the lower-valent *p*-element (here Ti or Zr) is the key interaction responsible for the formation of the *d*–*d* gap in these systems. On the other hand, the presence of the *sp*-valent element is crucial for the stability of these systems. A similar result has been reported from band structure calculations by the Korringa–Kohn–Rostoker (KKR) method made mainly for the Co-based compounds, but also for TiNiSn [10]. Among others, especially for the latter compound being a 18-valence electron system, the KKR type calculations with coherent potential approximation (CPA) have been published by Tobola et al. [11]. As many as nine valence bands below the Fermi level and a gap of an order of 0.4–0.9 eV have been reported.

So far the transport properties, except TiPtSn [5], have practically been not known for the Pt-based ternaries. Only a preliminary report on the temperature dependence of the resistivity in this group of compounds was presented in the literature, but without any deeper analysis of the observed dependences [2]. However, a careful analysis of magnetization isotherms performed for this family of compounds, being usually non-linear [12] at temperatures in the range from 1.9 to 300 K, has demonstrated that compounds studied with M = Th, Ti, Zr, and Hf are all diamagnetic. Furthermore, an application of nuclear magnetic resonance (NMR) of ^{47}Ti, ^{49}Ti, and ^{91}Zr quadrupolar nuclei has been turned out extremely useful in controlling the microscopic structure of half-Heusler, Pt-based phases [12]. On the other hand, no valuable information on structural properties in these APtSn phases could be obtained from the static NMR spectra of spin 1/2 ^{117}Sn.

Here we report the results of band structure calculations for all the three MPtSn phases (M = Ti, Zr, Hf) using the full-potential *ab initio* methods. For comparison we will discuss also the results reported in our previous paper on ThPtSn and UPtSn [13]. The calculated X-ray photoemission spectra for the valence band are compared with the experimental ones.

2. Method of calculations

In order to study electronic structure of MPtSn-type compounds (M = Ti, Zr, Hf) we used two full-potential *ab initio* methods. As the main one we have chosen the FPLO method [14], based on the LSDA [15]. The calculations were carried out for the lattice parameters: 6.160, 6.326, and 6.310 Å for TiPtSn, ZrPtSn, and HfPtSn, respectively. The computational method assumes different treatment of electrons, their orbitals may be classified according to the spatial extent of the radial functions and according to their occupation [14]. The configurations of atoms used in our calculations were the following: core + semicore electrons ($3s3p$) + valence electrons ($4s4p3d$) for Ti, core + semicore electrons ($4s4p$) + valence electrons ($5s5p4d$) for Zr, core + semicore electrons ($4f5s5p$) + valence electrons ($6s6p5d$) for Hf and Pt, and finally core + semicore electrons ($4s4p$) + valence electrons ($5s5p4d$) for Sn atoms.

The calculations were performed for the reciprocal space mesh containing 3091 points within the irreducible wedge of the Brillouin zone using the tetrahedron method [16] for integrations. The LSDA exchange-correlation potential was assumed in the form proposed by Perdew and Wang [17]. The self-consistent criterion was equal to 10^{-8} Ry for the total energy.

For complementary band structure calculations the FP-LMTO method implemented by the LmtART code [18, 19] was used. Details are described in Ref. [13].

The theoretical photoemission spectra were obtained from the calculated densities of electronic states (DOS) convoluted by Gaussian with a half-width equal to 0.3 eV and scaled using the proper photoelectronic cross-sections for partial states [20].

3. Experimental

The X-ray photoemission spectra were measured with monochromatized Al K_α radiation with photon energy of 1486.6 eV at room temperature using a PHI 5700/660 Physical Electronics Spectrometer. The energy of the electrons were analyzed by a hemispherical mirror analyzer with an energy resolution about 0.3 eV. The Fermi level, $E_F = 0$, was referred to the gold $4f_{7/2}$ binding energy at 84 eV. The samples were mechanically cleaned by scraping with a diamond file in a preparation chamber under high vacuum of 10^{-10} Torr. In the recorded spectra very small amount of oxygen and carbon was visible. No effects of oxidation during the data acquisition time were observed. The position of the peaks and the spin orbit splitting (SOS) was determined by use of MultiPak program from Physical Electronics, which makes very accurate fitting using Gauss and Lorentz curves and Shirley background [21]. In the text we present positions of the

lines and SOS with the accuracy of 0.1 eV. This is the experimental error for most samples (although the position of some peaks is determined with better accuracy).

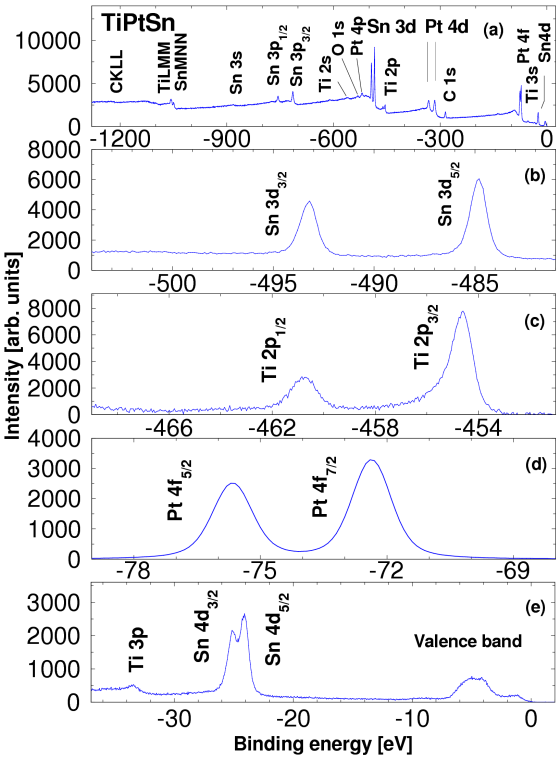

Fig. 1. The XPS for TiPtSn: in the wide energy range (a), the Sn $3d_{3/2}$, $3d_{1/2}$ lines (b), the Ti $2p_{3/2}$, $2p_{1/2}$ lines with a satellite peak due to TiO (c), the Pt $4f_{5/2}$, $4f_{7/2}$ lines (d), and the valence band spectrum (e).

The photoemission spectra for the three compounds MPtSn are collected in Figs. 1–3 and will be discussed in some details in the next section.

4. Results

4.1. TiPtSn

The X-ray photoemission spectra for TiPtSn are presented in Fig. 1. In the valence band spectrum (Fig. 1e) the hump seen at low binding energy (BE) results predominantly from *d*-electrons from Ti and Pt, and *p*-electrons from Sn, as can be estimated from the calculated DOS presented in Fig. 4 and the numbers of states (NOS) collected in Table. The split maximum at binding energy of about −5 eV is dominated by Pt *d*-electrons. The splitting of Sn $4d$ lines into Sn $4d_{5/2}$ (at BE −24.2 eV) and Sn $4d_{3/2}$ (at −25.1 eV) is equal to 0.9 eV, in reasonable agreement with the value of 1.05 eV found from the calculated band structure. At BE = −33.5 eV the Ti $3p$ contribution is fairly well resolved. Also the spin–orbit splitting of Ti $2p_{3/2}$ and Ti $2p_{1/2}$ lines, amounting to 6.2 eV (see Fig. 1c) is not far from the calculated value 5.76 eV. The broadening of the Ti $2p_{3/2}$ line at higher binding energy side (Fig. 1c) can be caused by a contamination with TiO. A trace of contamination with carbon (C $1s$ line at about −300 eV) and oxygen (O $1s$ line at about −530 eV) can be seen in Fig. 1a, as well as in the wide energy scan spectra for ZrPtSn (Fig. 2a) and HfPtSn (Fig. 3a). The Pt $4f_{5/2}$ and $4f_{7/2}$ lines (Fig. 1d) are nearly identical in all the systems studied here.

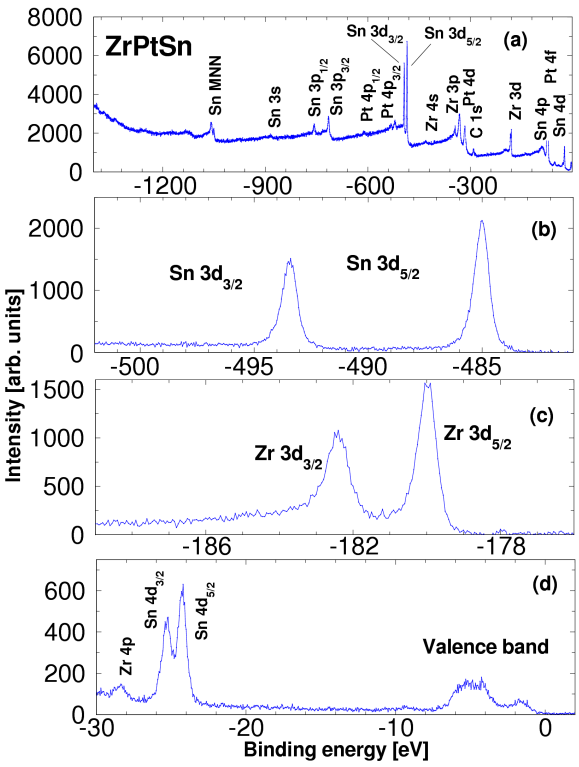

Fig. 2. The XPS for ZrPtSn: in the wide energy range (a), the split Sn $3d$ lines (b), the Zr $3d$ lines (c), and the valence band spectrum (d).

As a complementary data to Fig. 1 (and Figs. 2, 3 to follow) in Table there are summarized partial numbers of states in the two energy intervals (−5.5, −2.5) eV and (−1.5, 0) eV which accommodate majority of the occupied valence states. Besides these two regions another prominent feature is the characteristic separate subband (−10, −8) eV due mostly to *s*-electrons from Sn (the same features are observed in Figs. 2, 3 to follow).

4.2. ZrPtSn

The valence band (Fig. 2d) in the low binding energy range in ZrPtSn is similar to the one for TiPtSn. This is not surprising since the dominating feature, which is the split maximum around −5 eV, is again due to the Pt *d*-electrons. The lowest binding energy hump is in this case due to the *p*- and *d*-electrons from Zr and Pt, and the *p*-electrons of Sn. The lines Sn $4d_{5/2}$ (at −24.3 eV) and Sn $4d_{3/2}$ (at −25.3 eV) show spin–orbit splitting of

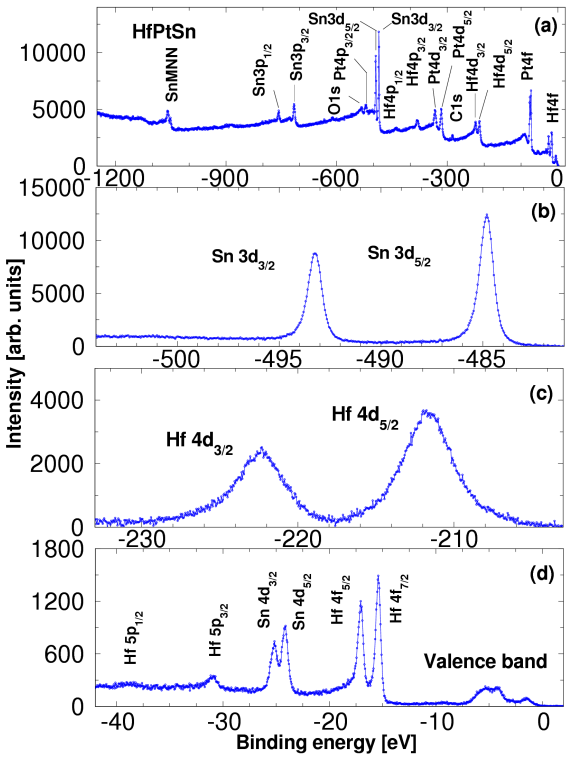

Fig. 3. The XPS for HfPtSn: in the wide energy range (a), the Sn $3d_{3/2}$, $3d_{5/2}$ lines (b), the Hf $4d_{3/2}$, $4d_{5/2}$ lines (c), and the valence band spectrum (d).

TABLE

Partial NOS of s, p, and d electrons contained in the two intervals of the binding energy (−5.5 eV, −2.5 eV) and (−1.5 eV, 0 eV), covering the two prominent features of the DOS's plots.

MPtSn	NOS(E_{12}) − NOS(E_{11}) $E_{11} = -5.5$ eV, $E_{12} = -2.5$ eV,			NOS(E_{22}) − NOS(E_{21}) $E_{21} = -1.5$ eV, $E_{22} = 0$ eV		
electrons	M = Ti	Pt	Sn	M = Ti	Pt	Sn
s	0.2218	0.2580	0.1274	0.0053	0.0059	0.0065
p	0.2919	0.2423	0.6402	0.0513	0.2149	0.2428
d	0.7970	6.1171	0.0125	0.9089	0.1383	0.0009
	M = Zr	Pt	Sn	M = Zr	Pt	Sn
s	0.3288	0.6002	0.1398	0.0525	0.0272	0.0276
p	0.3702	0.1787	1.1141	0.2148	0.5809	0.8161
d	0.9968	7.7519	0.0119	1.2048	0.4715	0.0014
	M = Hf	Pt	Sn	M = Hf	Pt	Sn
s	0.2559	0.3248	0.1182	0.0275	0.0213	0.0024
p	0.3378	0.1848	0.7994	0.2176	0.5344	1.9827
d	0.9059	7.2353	0.0116	1.0492	0.4133	0.0002

1.0 eV (the calculated value is 1.05 eV). At −28.4 eV the Zr $4p$ line can be identified. The core levels Zr $3d_{5/2}$ (at −179.9 eV) and Zr $3d_{3/2}$ (at –182.1 eV) are spin–orbit split by 2.2 eV. The Sn $3d$ lines are almost identical in all the three compounds reported here. In Fig. 2b the positions of Sn $3d_{5/2}$ and Sn $3d_{3/2}$ lines are at −484.9 eV and −493.4 eV, respectively. Their splitting is equal to 8.5 eV.

4.3. HfPtSn

The photoemission spectrum of HfPtSn in the energy range from the Fermi level to about −8 eV differs very little from the ones measured for the Ti- and Zr-based compounds. In this case the difference is that only the p- and d-states from Hf contribute to the hump mentioned above. The spin–orbit splitting of the Hf $4f$ and Hf $5p$ lines presented in Fig. 3d are 1.4 eV and 8.3 eV, which may be compared with the calculated ones, 1.74 eV and 7.94 eV, respectively. The splitting of the Sn $4d$ lines is 1.0 eV (calculated 1.05 eV), i.e. within an experimental error being the same as in the other members of the MPtSn family of compounds discussed here.

The calculated DOS are presented in Figs. 4–6. In the left parts site contributions are plotted, while in the right ones partial DOS's are drawn. There are some universal properties of the DOS for the series TiPtSn (Fig. 4), ZrPtSn (Fig. 5) and HfPtSn (Fig. 6). The most important feature is the energy gap occurrence at the Fermi level, equal to 0.747 eV, 1.117 eV and 1.087 eV for the Ti-, Zr- and Hf-based systems, respectively. Interesting also is the large, amounting about 2 eV, gap (roughly between −8 and −6 eV) between a subband strongly dominated by the Sn s-electrons and the lower part of the valence band.

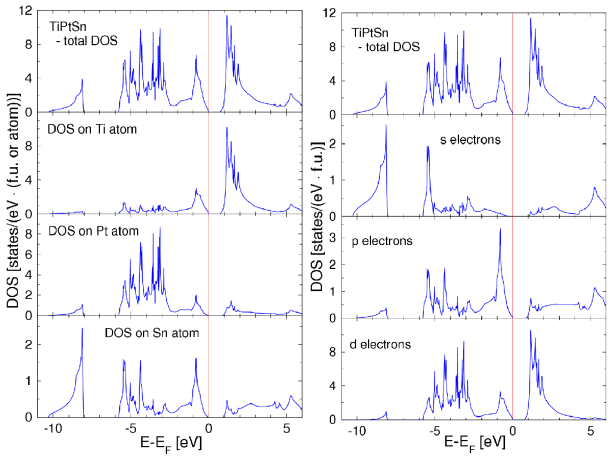

Fig. 4. The density of states (DOS) for TiPtSn and the site contributions for DOS in the left hand parts, the partial DOS in the right hand parts.

At first sight the plots in Figs. 4–6 look almost identical for energies below the Fermi level. However, some fine details are different. Note that around the Fermi level the curves are different mainly because of the high energy, unoccupied levels of d electrons. The reason of these similarities is simple — all the compounds studied here have the same crystallographic structure and analogous atomic environments. The Ti, Zr and Hf atoms, all belonging to the IV group have the same numbers of valence electrons: $3d^2 4s^2$, $4d^2 5s^2$ and $5d^2 6s^2$, respectively.

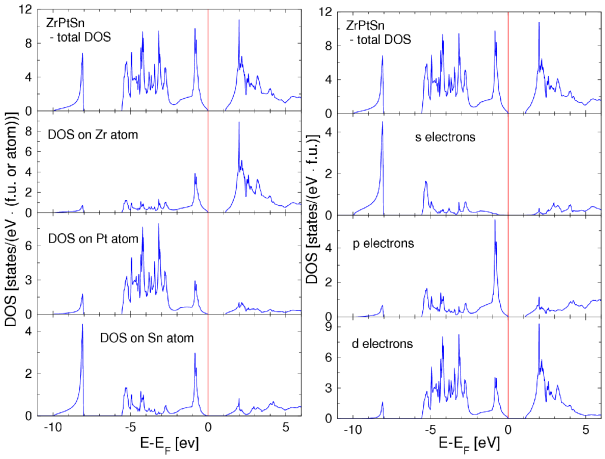

Fig. 5. DOS for ZrPtSn, details are like in Fig. 4.

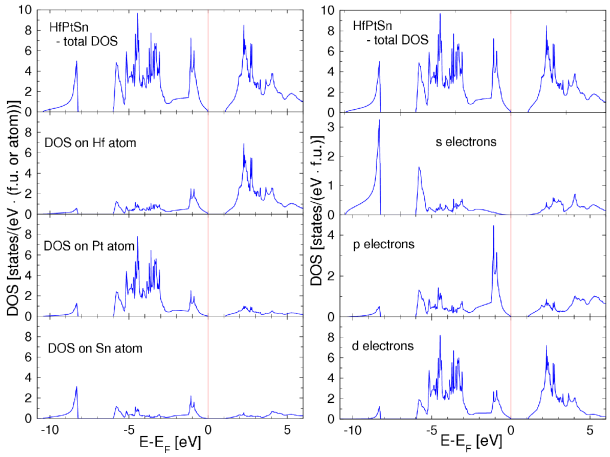

Fig. 6. DOS for HfPtSn.

Also, the leading contributions to DOS come from Pt and Sn atoms.

The calculated energy gaps at the Fermi level are much larger than those deduced [5] from the transport properties at high temperatures for some MPtSn compounds. In order to check the extent of a shrinking of the calculated gap with the increase in temperature due to the Fermi–Dirac distribution, the calculations at $T = 0$ K and room temperature were carried out by the LmtART program [19]. The results of FP-LMTO calculations by the LmtART code 6.50, using the Vosko et al. [22] exchange-correlation potential with the gradient corrections [23] for ZrPtSn and at 0 and 293 K are summarized as the total DOS plots in Fig. 7. The inset in Fig. 7 shows the vicinity of the gap in a narrow energy scale. The gap is 0.82 eV at $T = 0$ and about 0.66 eV at $T = 293$ K.

It should be pointed out that while band edges at $T = 0$ are sharp, then at $T = 293$ K long tails appear (however not seen in the extended scale of the ordinate axis in the inset in Fig. 7). The value of 0.66 eV for the gap has been determined as the distance between zeros

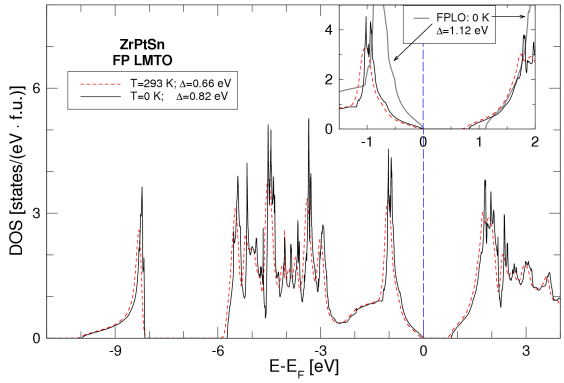

Fig. 7. The total DOS plots obtained by LmtART method at 0 and 293 K, the inset shows the gap region and comparison with results obtained by FPLO method at 0 K.

of DOS(E), with the accuracy of 10^{-7} states/(eV f.u.). However, linear extrapolation of the steep lines near the edges of the DOS plots to zero would give a value of about 0.76 eV.

5. Discussion

The most important part of the present study is comparison of the calculated photoemission spectra with the experimental ones. In the narrow gap semiconductors, as is the case in the MPtSn system studied here and in our earlier paper [13], the comparison with experiment is more difficult by the uncertainty of fixing the Fermi level properly. The calculations, resulting in Figs. 4–6, are done at zero temperature so the Fermi level is located at the top of the valence band. However, the photoemission experiments are performed at room temperature. Thus there exists some population of electrons in the conduction band, above the semiconducting gap and therefore the real chemical potential should be assigned to somewhere near the bottom of the conduction band. In consequence, Figs. 8a–c present a comparison of the measured X-ray photoemission spectroscopy (XPS) valence band with the two calculated spectra, one for the Fermi level at the bottom of the gap and the second corresponding to the Fermi level at the top of the gap.

The electronic structures of the system MPtSn for M = Ti, Zr, Hf have some features resembling the ones for M = Th, U reported in [13]. The obvious differences are due to the contributions of $5f$ electrons in the case of UPtSn, not present in Ti-, Zr-, Hf- and Th-systems. In the photoemission spectra of UPtSn $5f$ electrons contribute a pronounced peak just below the Fermi energy [13], no such features appear in the spectra for the other systems reported here and in [13]. The calculated energy gaps at the tops of the valence bands are very small (or even vanish for some choices of the exchange-correlation potential [13]) in Th- and U-systems [13], whereas for Ti-, Zr- and Hf- are of the order of 1 eV. The

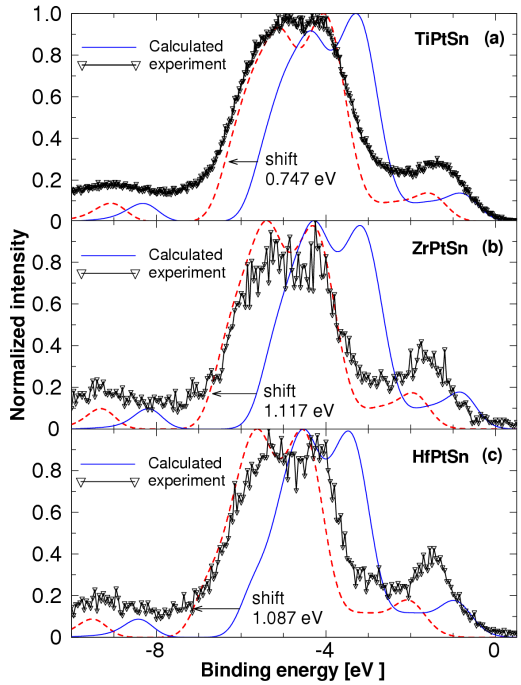

Fig. 8. Comparison of the measured and calculated valence band XPS for TiPtSn, ZrPtSn and HfPtSn. Points are experimental. The full lines are calculated taking the top of the valence band as the zero of the binding energy; the broken lines are for the energy zero at the bottom of the conduction band. The shift between the calculated lines is equal to the semiconducting gap.

shapes of the valence spectra in Fig. 8 and for Th in [13] are quite similar and differ from the one for U only by the absence of the U $5f$ peak at the Fermi level.

Acknowledgments

Financed from the science resources as a joint research program within scientific network "New materials and sensors for optoelectronics, informatics, energetics and medicine".

References

[1] W. Jeitschko, *Metall. Trans. A* **1**, 3159 (1970).

[2] F.G. Aliev, N.B. Brandt, V.V. Kozyrkov, V.V. Moshchalkov, R.V. Skolozdra, U.V. Stadnik, *Fiz. Nisk. Temp.* **13**, 498 (1987).

[3] B.A. Cook, J.L. Harringa, *J. Mater. Sci.* **34**, 23 (1999).

[4] C. Uher, J. Yang, S. Hu, *Phys. Rev. B* **59**, 8615 (1999).

[5] K. Ahilan, M.C. Benett, M.C. Aronson, N.E. Anderson, P.C. Canfield, E. Munoz-Sandoval, T. Gortenmulder, R. Hendrikx, J. Mydosh, *Phys. Rev. B* **69**, 245116 (2004).

[6] F.G. Aliev, *Physica B* **171**, 199 (1991).

[7] S. Ogut, K.M. Rabe, *Phys. Rev. B* **51**, 10443 (1995).

[8] A. Ślebarski, M. Orzechowska, A. Wrona, J. Szade, A. Jezierski, *J. Phys., Condens. Matter* **12**, 1262 (2000).

[9] B.R.K. Nanda, I. Dasgupta, *J. Phys., Condens. Matter* **15**, 7307 (2003).

[10] J. Pierre, R. Skolozdra, J. Tobola, S. Kaprzyk, C. Hordequin, M.A. Kouacou, I. Karla, R. Currat, E. Lelievre-Berna, *J. Alloys Comp.* **262-263**, 101 (1997).

[11] J. Tobola, J. Pierre, S. Kaprzyk, R.V. Skolozdra, M.A. Kouacou, *J. Phys., Condens Matter* **10**, 1013 (1998).

[12] A. Grykałowska, K. Wochowski, B. Nowak, *Intermetallics* **13**, 756 (2005).

[13] A. Szajek, J.A. Morkowski, A. Bajorek, G. Chełkowska, R. Troć, *J. Magn. Magn. Mater.* **281**, 281 (2004).

[14] FPLO-5.00-18 [improved version of the original FPLO code by K. Koepernik, H. Eschrig, *Phys. Rev. B* **59**, 1743 (1999)]; `http://www.FPLO.de` .

[15] H. Eschrig, *The Fundamentals of Density Functional Theory*, 2nd ed, Edition am Gutenbergplatz, Leipzig 2003.

[16] P. Blöchl, O. Jepsen, O.K. Andersen, *Phys. Rev. B* **49**, 16223 (1994).

[17] J.P. Perdew, Y. Wang, *Phys. Rev. B* **45**, 13244 (1992).

[18] S.Y. Savrasov, D.Y. Savrasov, *Phys. Rev. B* **46**, 12181 (1992).

[19] S.Y. Savrasov, *Phys. Rev. B* **54**, 16470 (1996).

[20] J.J. Yeh, I. Lindau, *At. Data Nucl. Data Tables* **32**, 1 (1985).

[21] D.A. Shirley, *Phys. Rev. B* **5**, 4709 (1972).

[22] S.H. Vosko, L. Wilk, M. Nusair, *Can. J. Phys.* **58**, 1200 (1980).

[23] J.P. Perdew, K. Burke, M. Ernzerhoff, *Phys. Rev. Lett.* **77**, 3865 (1996); ibid. **78**, 1396 (1997).